Model calculations on the band structures of one-dimensional mixed donor-acceptor systems

Michael C. Böhm
Institut für Organische Chemie der Universität Heidelberg, D-6900 Heidelberg, West Germany

Helmut Vogler
Abteilung für Organische Chemie, Max-Planck-Institut für Medizinische Forschung, D-6900 Heidelberg, West Germany

(Received 9 December 1982)

The band structures of one-dimensional donor-acceptor (*D-A*) stacks have been studied by means of the crystal-orbital (CO) formalism based on the tight-binding approximation. The model polymers of the present study are composed of quinhydrone moieties (10 and 11) where the donor and acceptor groups show either a parallel or a perpendicular orientation. These idealized systems have been adopted as models for *D-A* polymers in the recently synthesized class of *D-A* phanes. The strength of the *D-A* interaction has been modified due to alterations of the *D-A* distances within the unit cells and due to modifications in the effective electronegativity of the active groups (hydroxyl and carbonyl). The computational framework is a semiempirical intermediate neglect of differential overlap (INDO) CO formalism with a variable model Hamiltonian that allowed the simulation of the different types of *D-A* interactions (weak versus strong *D-A* pairs). An insulator-metal transition is predicted in the 0° arrangement of 10 for short *D-A* distances and larger differences in the electronegativities of both fragments. The 90° conformation shows an avoided crossing between the highest filled and the lowest unfilled $\epsilon(k)$ curves. This leads to a finite band gap for all studied interaction conditions. The band structures, the charge transfer in the *D-A* stacks, and the excited-state properties of 10 and 11 are analyzed as a function of the *D-A* geometry (distance, mutual orientation) and as a function of the strength of the *D-A* pairs. Semiquantitative solid-state models are compared with the INDO CO data, synthetic strategies for the design of *D-A* phanes with small (vanishing) band gaps are formulated, and various solid-state effects encountered in related low-dimensional *D-A* systems are briefly discussed.

I. INTRODUCTION

The physical and chemical properties of quasi-one-dimensional (1D) organic solids with donor (*D*) and acceptor (*A*) moieties as the molecular building blocks have found considerable interest in the past two decades.[1-5] On the basis of the mutual arrangement of the *D* and *A* units, two topologically different solid-state modifications can be discriminated in the family of the organic charge-transfer (CT) systems: segregated stacks where all *A*'s and *D*'s crystallize in separate face-to-face columns, as well as mixed stacks with an alternating arrangement of the donor and acceptor moieties.

Segregated stacks:

$$\cdots A^{q-}A^{q-}A^{q-}\cdots$$

and

$$\cdots D^{q+}D^{q+}D^{q+}\cdots .$$

Mixed stacks:

$$\cdots A^{q-}D^{q+}A^{q-}D^{q+}A^{q-}D^{q+}\cdots .$$

In the latter class of the low-dimensional materials, *D-A* phanes with well-defined separations and orientations between *D* and *A* have been studied extensively.[6-10] A collection of *D-A* phanes that have been synthesized recently is displayed in Fig. 1. Owing to the close correspondence to the historically important quinhydrone complex, the [2.2] paracyclophanes 1 and 2 were the objects of a large amount of experimental investigations. 1 and 2 differ in the *D-A* orientation (pseudogeminal, 1; pseudo-ortho, 2)

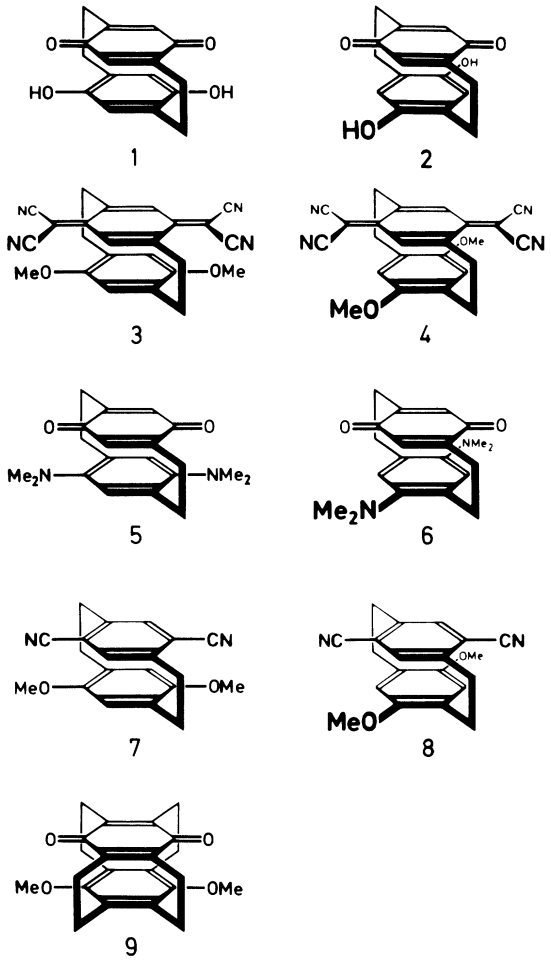

FIG. 1. Representative collection of *D-A* phanes 1–9. ("Me" is an abbreviation for the methyl group.)

and are characterized due to different optical-absorption spectra.[6,7]

Theoretical approaches to rationalize the electronic structures of the aforementioned CT systems have been developed for both types of 1D materials. The theoretical activities in the area of the segregated stacks exceed the solid-state approaches developed for the mixed systems with alternating donor and acceptor units. The computational tools employed in the class of the segregated systems span a range from simple models that can be solved analytically for small unit-cell dimensions (e.g., one atom and one basis function per cell) to classical crystal-orbital (CO) calculations derived in the framework of the tight-binding formalism.[11,12] Most of the analytically soluble studies are based on some variants of the Hubbard Hamiltonian.[13] Various groups have used this model Hamiltonian in tight-binding calculations on infinite systems.[14,15] Soos and coworkers have adopted this approach to analyze mixed *D-A* stacks.[16,17]

Band-structure calculations have been reported for the infinite neutral tetracyanoquinodimethane and tetrathiafulvalene stacks; the CO calculations are either based on semiempirical model Hamiltonians or on the *ab initio* formalism.[18–21] This variety in the theoretical approaches is not found in the class of the mixed stacks that are characterized by large unit-cell dimensions. Present solid-state investigations on these infinite systems are restricted to conceptions based on the Hubbard Hamiltonian.[22–25] On the other hand, various theoretical studies[26–30] have been published for the molecular building blocks $A^{q-}D^{q+}$ that are often related to the classical contributions of Mulliken on weak CT complexes.[31] To our knowledge, band-structure calculations that are based on the CO formalism have not been published for low-dimensional *D-A* systems that belong to the latter topology.

It is the purpose of the present contribution to elucidate those factors that determine the electronic structure (insulating and semiconducting versus metallic properties) of mixed $A^{q-}D^{q+}$ stacks in the solid state. We have adopted model polymers that are derived from the two [2.2] paracyclophanes 1 and 2 with different orientations of the donor and acceptor moieties (see Fig. 2). Our employed model systems 10 and 11 are composed by quinhydrone units where the donor and acceptor functions in the two π units show a parallel orientation (10) or are rotated by 90° (11). The first geometry corresponds exactly to the pseudogeminal [2.2] paracyclophane orientation (1), while the perpendicular arrangement is closely related to the pseudo-ortho derivative 2. We have neglected the bridging $-CH_2-CH_2-$ units in the model calculations in order to reduce the dimensions of the unit cells and thus to save computer

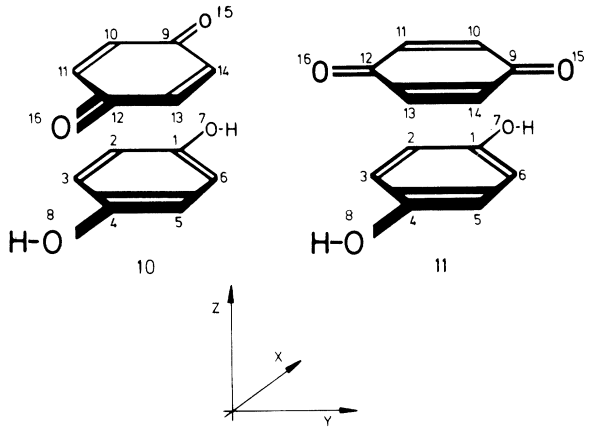

FIG. 2. Quinhydrone units 10 and 11 that correspond to the unit cells employed in the INDO CO calculations. The donor and acceptor groups are parallel in 10 and perpendicular in 11. The atomic numbering scheme is displayed in both *D-A* fragments.

time. The photoelectron spectra of a large number of phane derivatives have shown[32] that this is no severe restriction as the energetic effects of nuclear deformations due to the $-CH_2-CH_2-$ bridges and "through-bond"[33] interaction largely compensate each other. To reduce the geometrical degrees of freedom we always assumed strictly planar π units in the donor and acceptor systems. Two different separations between *A* and *D* have been adopted in the 1D models 10 and 11. We have employed a long *D-A* separation of 3.0 Å (10*a*,11*a*) as well as a short distance of 2.6 Å (10*b*,11*b*). X-ray investigations on different cyclophanes have shown that the first value is found conveniently in [2.2] paracyclophane derivatives. The short separation is an absolute minimum in the class of phanes, and it has been detected in superphane, where the π units are coupled via six $-CH_2-CH_2-$ bridges.[34-36]

The theoretical framework of the present investigation is the CO model that has been implemented into a semiempirical intermediate neglect of differential overlap (INDO) Hamiltonian.[37] The zero-differential overlap (ZDO) operator has been designed to reproduce the results of time-consuming *ab initio* calculations at low computational expense in the case of organic and organometallic systems.[38] In order to study the band structure as a function of the coupling strength between the donor and acceptor units, we have modified the effective electronegativities of the carbonyl groups in *A* and the hydroxyl groups in *D* within small intervals to mimic both weak and strong *D-A* pairs in the 1D stacks. This strategy is closely related to the aforementioned theoretical solid-state approaches based on the Hubbard Hamiltonian in which different values for on-site Coulomb elements and transfer integrals have been used. Molecular studies with variable Hamiltonians have been published at various degrees of sophistication to understand the mutual dependence of ionization and excitation energies as well as the importance of electron correlation as a function of the model space spanned by the effective Hamilton operator.[39-45] Different molecular regimes (valence-bond limit versus molecular-orbital limit) have been simulated due to modifications in the analytic shape of the two-electron interaction and via variations in the one-electron coupling.

In the present CO investigations, on the other hand, we are interested in a common one-particle CO space for different donor and acceptor capabilities in the active molecular frames. Therefore it is not suitable to modify either the two-electron part of the model Hamiltonian or the one-electron coupling (resonance integrals). Thus we have restricted our systematical modifications in the ZDO operator to the atomic-core integrals of the donor and acceptor groups that determine the basis energies (electronegativities) of the atomic centers or molecular fragments (see the next section).

The theoretical background of the CO formalism as well as the physical nature of the model operator are shortly discussed in the next section. The band structures of the *D-A* polymers 10 and 11 for different coupling conditions are analyzed in Sec. III. In order to link the findings derived in the CO formalism with current theoretical results based on descendants of the Hubbard Hamiltonian, we try, furthermore, to compare critically, but rather qualitatively, some of the INDO CO results with simplified four-electron four-orbital models (see Sec. IV).

II. COMPUTATIONAL FRAMEWORK

The CO formalism has been described in much detail in the literature.[11] A thorough derivation of the matrix elements of the CO Fock operator in the present INDO approximation is given in Ref. 37. Thus only the most important aspects of the tight-binding method are shortly reviewed in this paragraph. The CO's are determined by means of the complex Hermitian pseudoeigenvalue problem defined in Eq. (1):

$$F(k)C(k)=\epsilon(k)C(k)\ , \tag{1}$$

which is already the ZDO-adapted form of the Hartree-Fock (HF) self-consistent field (SCF) scheme in the CO formalism. Equation (1) must be solved self-consistently point by point in the (reciprocal) k space within the first Brillouin zone. The Fock matrix $F(k)$ is determined by the Fourier sum

$$F(k)=\sum_{j=-\infty}^{+\infty}\exp(ijk)F(j)\ , \tag{2}$$

where j is a cell index. $F(k)$ can be decomposed into a one-electron core operator $H(k)$ and the two-electron part $G(k)$,

$$F(k)=H(k)+G(k)\ , \tag{3}$$

$$H(k)=H(0)+\sum_{\substack{j=-\infty\\ j\neq 0}}^{+\infty}\exp(ijk)H(j)\ , \tag{4}$$

$$G(k)=G(0)+\sum_{\substack{j=-\infty\\ j\neq 0}}^{+\infty}\exp(ijk)G(j)\ , \tag{5}$$

where $k=0$ labels the reference cell in the origin. The contributions to $H(0)$ that contain only coordinates (electronic and nuclear) of the reference cell are defined in Eqs. (6) and (7):

$$H(0)^{AA'}_{\mu\mu}=U^{AA}_{\mu\mu}+\sum_{\substack{B\\B\neq A}}V^{AB}_{\mu B}\,, \tag{6}$$

$$H(0)^{AB'}_{\mu\nu}=\beta^{AB}_{\mu\nu}\,, \tag{7}$$

where μ and ν are basis functions of the atomic orbitals and A and B label atomic centers:

$$U^{AA}_{\mu\mu}=(\mu^A\,|\,[-\tfrac{1}{2}\nabla^2-V_A]\,|\,\mu^A)\,, \tag{8}$$

$$V^{AB}_{\mu B}=(\mu^A\,|\,V_B\,|\,\mu^A)\,, \tag{9}$$

$$\beta^{AB}_{\mu\nu}=(\mu^A\,|\,[-\tfrac{1}{2}\nabla^2-V_A-V_B]\,|\,\nu^B)\,. \tag{10}$$

$U^{AA}_{\mu\mu}$ is the atomic-core operator, the energy of the μth electron in the field of the core of the Ath atom. $U^{AA}_{\mu\mu}$ thus determines the basis energy (electronegativity) of the atomic orbital (AO) μ at the Ath center. Experimental $U^{AA}_{\mu\mu}$ numbers are available from the atomic spectra of the various elements[46] and have been adopted in the present INDO CO model. $V^{AB}_{\mu B}$ is the electron-core interaction between the μth AO at center A and the core of atom B, while $\beta^{AB}_{\mu\nu}$ is the resonance integral between the μth AO at A and AO ν at B. The detailed formulas as well as the remaining matrix elements of the crystal Hamiltonian are given in Ref. 37.

The two-electron integrals of the INDO CO operator have been either determined on the basis of experimental quantities (one-center elements)[38] or via the semiempirical Dewar-Sabelli-Ohno-Klopman[47] relation

$$\gamma^{AB}_{\mu\nu}=(\mu^A\mu^A\,|\,r_{12}^{-1}\,|\,\nu^B\nu^B)$$
$$=(\mu^A\mu^A\,|\,\nu^B\nu^B)=\{R^2_{AB}+0.25[(\mu^A\mu^A\,|\,\mu^A\mu^A)^{-1}+(\nu^B\nu^B\,|\,\nu^B\nu^B)^{-1}]^2\}^{-1/2}\,, \tag{11}$$

where the two-center two-electron integrals are related to the corresponding one-center elements. Electron-electron interaction and screening due to the atomic cores is thus partially taken into account even in the one-determinantal formalism of the HF approximation.

The $F(k)$ matrices are coupled via the charge-density—bond-order matrices

$$P_{\mu\nu}(j-j')=(c/2\pi)\int_{-\pi/c}^{+\pi/c}\sum_i c^*_{i\mu}(k)_{i\nu}(k)\exp[ik(j-j')]\Theta(\epsilon_F-\epsilon(k)_i)dk\,, \tag{12}$$

where c is the unit-cell dimension, ϵ_F is the Fermi energy, and Θ is the Heaviside step function. Equations (3) and (12) correspond to a nonparamagnetic polymer which has its molecular analogy in closed-shell systems. The total energy of the 1D stack is defined in Eq. (13), and has been normalized to one unit cell,

$$E=(c/2\pi)\int_{-\pi/c}^{+\pi/c}\sum_i[c_i^*(k)H(k)c_i(k)+\epsilon(k)_i]\times\Theta(\epsilon_F-\epsilon_i(k))dk+E_{\text{core}}\,, \tag{13}$$

where E_{core} symbolizes the repulsion between the atomic cores.

To modify the donor and acceptor strength in the model polymers 10 and 11, we have varied the atomic-core integrals $U^{AA}_{\mu\mu}$ at the active centers O_7,O_8,H_7,H_8 (donor), and C_9,C_{12},O_{15},O_{16} (acceptor, see Fig. 2) according to Eqs. (14) and (15),

$$U^{AA}_{\mu\mu}(\text{acceptor})=U^{AA}_{\mu\mu}-\Delta U\,, \tag{14}$$

$$U^{AA}_{\mu\mu}(\text{donor})=U^{AA}_{\mu\mu}+\Delta U\,, \tag{15}$$

while all other $U^{AA}_{\mu\mu}$ elements were kept fixed to their standard values. In the model calculations on 10 and 11 we have modified ΔU in an interval between 0 eV (standard) to 8 eV. To get some insight into the energetic width of the effective electronegativities we have summarized some representative experimental $U^{AA}_{\mu\mu}$ parameters in Table I.[46]

The INDO CO equations have been solved at ten points in the first Brillouin zone; the lattice sums (index j) have been extended to the fifth-nearest neighbors. To guarantee iterations to the true energy minimum of the corresponding polymers we have done HF SCF CO calculations on various occupation patterns for the energy bands of 10 and 11 (in some model calculations, insulating and metallic states). In the subsequent discussion we have always employed those INDO CO results derived for the external conditions (donor and acceptor separation, mutual orientation, effective electronegativity in the hydroxyl and carbonyl fragments) that are lowest in energy.

For the determination of the density of states $N(E)$, we have adopted a classical definition.[48,49] The dispersion curves for the D-A systems have been fitted by means of fourth-order polynomials that have been calculated via a least-squares formalism to the ten $\epsilon(k)$ points per band. The $N(E)$ histograms were constructed with the aid of 30 000 data points for each dispersion curve. A common nor-

TABLE I. Representative set of atomic-core integrals $U_{\mu\mu}^{AA}$ employed in the present CO Hamiltonian; the $U_{\mu\mu}^{AA}$ parameters have been derived on the basis of spectroscopic data (Ref. 46) and are associated with the complete neglect of differential overlap (CNDO) variant of the ZDO operator. The corresponding INDO elements are slightly modified by means of higher multipole components in the one-center two-electron integrals encountered in the INDO approximation (Ref. 38). All values in eV.

Atom	U_{ss}^{AA}	U_{pp}^{AA}
H	−13.595	
Li	−4.999	−3.673
Be	−15.543	−12.280
B	−30.371	−24.702
C	−50.686	−41.530
N	−70.093	−57.848
O	−101.306	−84.284
F	−129.544	−108.933
Si	−36.494	−30.375
P	−56.230	−42.310
S	−66.768	−58.008
Ge	−35.844	−29.973
As	−50.151	−44.485
Se	−66.005	−57.927

malization constant has been used for all $N(E)$ plots in order to allow a critical comparison of the density-of-states distribution in the different model polymers.

The geometrical parameters of Ref. 50 have been employed in the INDO CO calculations on the phane models 10 and 11. The averaged C-C distances in the donor ring amount to 1.40 Å, while a C-O separation of 1.36 Å has been assumed. In the acceptor moiety the following bond lengths have been used: $d_{C_9C_{10}}=1.46$ Å, $d_{C_{10}C_{11}}=1.34$ Å, $d_{C_9O_{15}}=1.22$ Å. Standard values of 1.08 Å for the C—H bonds and 0.96 Å for the hydroxyl bonds have been accepted.[51] The hydroxyl groups are in the plane of the π ring. The symmetry of the *D-A* polymers 10 and 11 is C_2. The unit-cell dimension c in 10*a* and 11*a* amounts to 6 Å; all *D-A* separations are identical. This stacking pattern has been detected in x-ray investigations on the *D-A* phanes 1 and 2. In the case of 10*b* and 11*b* we have used a unit-cell parameter of 5.6 Å; the polymer is characterized due to an alternancy in the formal *D-A* distances (2.6-Å intracell interaction versus 3.0-Å intercell coupling). The effective masses for injected holes in the valence bands and for injected electrons in the conduction bands for insulating model polymers have been calculated by means of the simple parabolic energy wave vector connection shown in Eq. (16),[52]

$$m_{h(e)}=\frac{\hbar^2\pi^2}{2c^2\Delta\epsilon}\ , \tag{16}$$

where $\Delta\epsilon$ is the width of the valence band or conduction band, respectively.

To simplify a critical discussion of the INDO CO results on the *D-A* polymers 10 and 11 it should be mentioned that the computational band-structure data are subject to the convenient theoretical shortcomings that are encountered in HF SCF CO calculations. Thus it is well known that band gaps predicted in the *ab initio* CO framework are too large in comparison to experimentally derived gaps.[53] This behavior must be traced back to the neglect of electron correlation in the HF approximation and to failures of the HF SCF formalism to describe unoccupied one-electron functions (orbitals in molecules, band states in polymers) due to a V_N (N electrons) potential instead of the correct $V_{(N-1)}$ potential.[54] The present ZDO operator, on the other hand, is an effective Hamiltonian with dressed two-electron integrals [see Eq. (11)] that lead to a renormalization of the $1/r_{12}$ influence as well as to a renormalized one-particle regime (filled and unfilled bands). The INDO CO band gaps (with the standard parametrization of the ZDO operator) are significantly smaller than *ab initio* gaps derived with bare two-electron integrals.[37] Therefore we can expect that theoretically determined band gaps in the *D-A* polymers are of reliable accuracy even in the HF formalism due to the reduction of the $1/r_{12}$ influence and due to the leveling of the $V_N/V_{(N-1)}$ problem.

Furthermore, it must be mentioned that all INDO CO calculations are restricted to CO solutions that are nonparamagnetic in order to avoid the difficulty of comparing restricted (closed-shell systems in the area of molecular quantum chemistry) and unrestricted (paramagnetic, open-shell behavior in the molecular domain) solutions in the tight-binding formalism. Additionally, it should be adduced that various objections have been advanced against the physical justification of the HF SCF CO formalism, especially for metallic systems.[55]

Nevertheless, it should be clear that the theoretical shortcomings of the CO method are no real significant restrictive obstacle in the following analysis. In the first place, we are interested in gradual changes in the band-structure calculations as a function of the variable donor and acceptor capabilities. Such a comparison is, of course, feasible in a model that forms a unique physical background, although the method is subject to certain conceptual shortcomings. In the second place, we have selected some idealized model polymers. It is not the primary aim of the present study to explain specific ex-

perimental results encountered in real low-dimensional *D-A* phanes, but we are interested to elucidate and rationalize basic principles and interaction patterns that determine the solid-state properties in a large class of compounds.

III. RESULTS OF THE INDO CO MODEL CALCULATIONS

In Table II the charge separations ΔQ between the donor and acceptor moieties in 10*a*, 10*b*, 11*a*, and 11*b*, together with the atomic net charges q_i,[56] are displayed as a function of the effective electronegativity of the active groups ($0 \leq \Delta U \leq 8$ eV). Graphical representations are shown in Figs. 3–5. The variation of ΔQ as a function of ΔU is given in Fig. 3. The modifications of the individual atomic net charges q_i for the polymers 10*b* and 11*b*, respectively, with the short *D-A* distances (2.6 Å) are shown in the next two figures. It is seen that the charge separations between the donors and acceptors are quite significant even for the standard parametrization ($\Delta U = 0$ eV) of the INDO CO Hamiltonian. The ΔQ values are found in an interval between 0.1680 (11*a*) and 0.3316 (10*b*). The CT is larger in the two 0° polymers and is enhanced with decreasing *D-A* separations. The ΔQ dependence is less marked for the interval $0 \leq \Delta U \leq 4$ eV, while it is dramatically enhanced for ΔU elements that exceed 4 eV. The relative sequence of the CT in the series 10*a*, 10*b*, 11*a*, and 11*b* is conserved in the first interval; it is, however, modified at $\Delta Q = 6$ eV where the most efficient charge shifts are diagnosed in the two 0° polymers 10*a* and 10*b*. The ΔQ width is largest at this point (for 11*a*, 0.6179; for 10*b*, 1.4512). The graduation of the ΔQ values between the 0° polymers on one side and the 90° modifications on the other side is reduced if the ΔU parameters in the donor and acceptor units are enlarged to 8 eV. The calculated ΔQ elements span a range from 1.6557 (11*a*) to 2.1985 (10*b*). The ΔQ width has a pronounced maximum at $\Delta U = 6$ eV ($\Delta\Delta Q = 0.8333$); it is, of course, reduced at $\Delta U = 0$ eV ($\Delta\Delta Q = 0.1636$), but it is also significantly diminished at $\Delta U = 8$ eV ($\Delta\Delta Q = 0.4326$).

The most important charge redistributions at the atomic sides can be identified in Table II. The graphical presentations in Figs. 4 and 5 show that the variations of the q_i values are not restricted to the active donor (hydroxyl) and acceptor (carbonyl) groups. Substantial electronic rearrangements are found at all π centers of the two ring systems. It is immediately recognized that the CT in 10*b* (0°) is more efficient in comparison to 11*b* (90° conformation). The electron density in the donor moiety is reduced at $O_7 = O_8$ (largest variation), but also at the carbon centers $C_2 = C_5$ and $C_3 = C_6$.

The opposite transfer path is encountered at the C centers $C_1 = C_4$ which are adjacent to the hydroxyl groups. A strong polarization of the π system is predicted in the quinone fragment. The electron density in the carbonyl-group moieties C_9/O_{15} and C_{12}/O_{16} is dramatically enhanced. The variations at the carbon centers C_9/C_{12} exceed the charge accumulation at the electronegative oxygen atoms O_{15} and O_{16}. The increase of electron density at the carbonyl groups as a function of ΔU is accompanied by a simultaneous reduction of the atomic population at the remaining carbon sites C_{10}, C_{11}, C_{13}, and C_{14}. The magnification of the donor and acceptor abilities thus has two effects on the electronic structures of the low-dimensional systems 10*a*–11*b*: (a) enlarged charge separation between the *D-A* pairs with increasing ΔU (interfragment); (b) strong polarization (intrafragment redistribution) in the π units.

Important band-structure data for the model systems 10*a*–11*b* as a function of ΔU are collected in Table III. The positions of the valence and conduction bands are given at the zone center (point Γ) and at the edge of the Brillouin zone (point X). $\Delta\epsilon$ is the associated bandwidth which is not necessarily identical with $|\epsilon(0) - \epsilon(\pi/c)|$. The effective masses ($m_h$ and m_e) have been calculated by means of Eq. (16). In the last columns we have summarized the forbidden band gaps, the types of the gaps, as well as the positions at the top (bottom) of the valence (conduction) bands. The dispersion curves for the 23 highest filled bands and for the 6 lowest unfilled bands are displayed in Figs. 6–9 (Fig. 6, 10*a*; Fig. 7, 11*a*; Fig. 8, 10*b*; Fig. 9, 11*b*). A representative density-of-states diagram (10*b*) is shown in Fig. 10; the energy grid employed in the $N(E)$ plots amount to 0.3 eV.

The model system 10*a* (0°, 3 Å) has a forbidden band gap for each value of ΔU. It is seen that the gap of 6.31 eV ($\Delta U = 0$ eV) is reduced to 5.27 and 2.95 eV, respectively ($\Delta U = 2$, 4 eV), with enlarged donor and acceptor capabilities. The smallest gap is found for a ΔU element of 4 eV; it is enlarged if ΔU is further increased (3.18 and 4.75 eV for $\Delta U = 6$ and 8 eV, respectively). The gaps are indirect for the two extreme ΔU points considered in this study ($\Delta U = 0$ eV, $\Delta U = 8$ eV), direct gaps at the edge of the Brillouin zone are predicted for the remaining ΔU potentials. The forbidden gap for $\Delta U = 0$ is found between point X of the valence band and point Γ of the conduction band; the opposite behavior is encountered in the case of $\Delta U = 8$ eV. The effective masses for injected holes (m_h) and injected electrons (m_e) are reduced with decreasing band gaps. Both quantities are closest to the free-electron behavior ($m_f = 1$) in the system with the

TABLE II. Calculated charge separations (ΔQ) between donor and acceptor units and atomic net charges in the two π moieties according to the semiempirical approach for the *D-A* models 10*a*–11*b*. The net charges of the H atoms at the carbon centers are not summarized in the table.

r_{AB} (Å)	α	ΔU (eV)	ΔQ	$C_1=C_4$	$C_2=C_5$	$C_3=C_6$	$O_7=O_8$	$H_7=H_8$	$C_9=C_{12}$	$C_{10}=C_{13}$	$C_{11}=C_{12}$	$O_{15}=O_{16}$
3.0	0°	0.0	0.2073	0.358	−0.182	−0.245	−0.471	0.345	0.497	−0.185	−0.215	−0.513
		2.0	0.3111	0.293	−0.175	−0.243	−0.353	0.349	0.286	−0.080	−0.110	−0.547
		4.0	0.5499	0.224	−0.159	−0.234	−0.184	0.354	0.042	0.028	−0.002	−0.613
		6.0	0.9738	0.134	−0.062	−0.167	0.211	0.371	−0.426	0.155	0.132	−0.826
		8.0	2.0011	−0.089	−0.005	−0.118	0.597	0.384	−0.921	0.380	0.362	−0.967
3.0	90°	0.0	0.1680	0.325	−0.171	−0.233	−0.504	0.344	0.506	−0.177	−0.208	−0.528
		2.0	0.2446	0.217	−0.143	−0.207	−0.405	0.346	0.296	−0.072	−0.104	−0.545
		4.0	0.3735	0.095	−0.104	−0.174	−0.285	0.349	0.074	0.034	0.002	−0.575
		6.0	0.6179	−0.053	−0.037	−0.128	−0.125	0.354	−0.179	0.144	0.111	−0.633
		8.0	1.6557	−0.150	0.186	−0.171	0.274	0.379	−0.721	0.308	0.270	−0.833
2.6	0°	0.0	0.3316	0.416	−0.174	−0.265	−0.467	0.349	0.514	−0.204	−0.232	−0.551
		2.0	0.4868	0.362	−0.165	−0.261	−0.339	0.353	0.300	−0.100	−0.132	−0.600
		4.0	0.8629	0.295	−0.142	−0.239	−0.212	0.359	−0.067	0.059	0.026	−0.698
		6.0	1.4512	0.134	−0.069	−0.173	0.201	0.370	−0.527	0.243	0.219	−0.860
		8.0	2.1985	−0.055	0.036	−0.113	0.617	0.383	−1.074	0.433	0.424	−1.005
2.6	90°	0.0	0.2406	0.388	−0.053	−0.392	−0.512	0.348	0.536	−0.297	−0.104	−0.581
		2.0	0.3812	0.276	−0.013	−0.346	−0.411	0.351	0.319	−0.202	0.000	−0.609
		4.0	0.5920	0.149	0.040	−0.289	−0.288	0.354	0.083	−0.102	0.103	−0.653
		6.0	0.9312	−0.005	0.111	−0.204	−0.121	0.357	−0.197	0.018	0.202	−0.723
		8.0	1.7659	−0.206	0.240	0.014	0.127	0.372	−0.673	0.318	0.162	−0.854

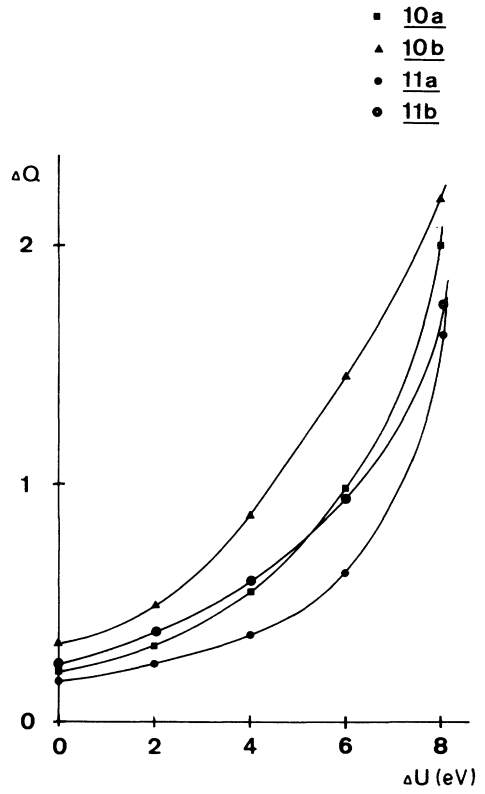

FIG. 3. Charge separations ΔQ between D and A in 10*a*, 10*b*, 11*a*, and 11*b* as a function of ΔU (variation of the effective electronegativity in the donor and acceptor groups).

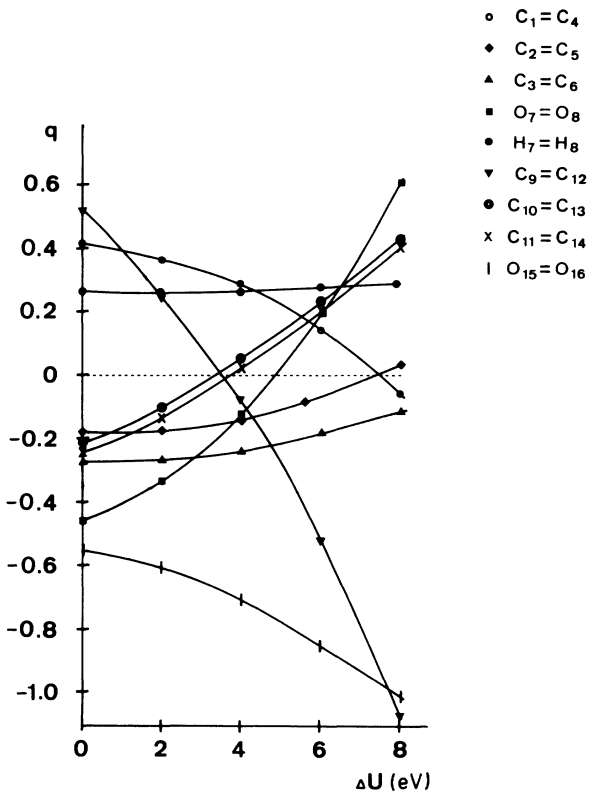

FIG. 4. Variation of the atomic net charges q_i in 10*b* as a function of ΔU. The labels at the various q_i curves are explained on the extreme right-hand side of the figure. The q_i modification of the H atoms in the six-membered rings is not shown (exception: H in the hydroxyl groups).

minimum band gap.

The CO amplitudes in the valence and the conduction bands of 10*a* at the Γ and X points are displayed in Fig. 11 for three characteristic values of ΔU [$\Delta U=0$ eV (top), $\Delta U=2$ eV (middle), and $\Delta U=6$ eV (bottom)]. The photon absorption from the top of the valence band ($k=\pi/c$) to the bottom of the conduction band ($k=0$) is characterized due to an intermixing of a CT from the hydroquinone donor to the acceptor and a local excitation in the donor fragment. This indirect absorption is nearly degenerate (0.06-eV difference) with a direct process at the center of the Brillouin zone. The excitation corresponds to a transition from a dative *D-A* structure to the "no-bond" state in the terminology of Mulliken.[31] The CO amplitudes at the zone center are strongly localized in the D and A fragments for ΔU elements of 2 and 4 eV (see Fig. 14). The direct photon absorptions are therefore typical CT processes $D\rightarrow A$ in contrast to the $\Delta U=0$ eV case. The localization properties of the CO's are substantially changed in the 1D systems where the difference in the electronegativities is furthermore enhanced. The CO amplitudes in the valence band (point X) are localized in the quinone moieties, while the zone-

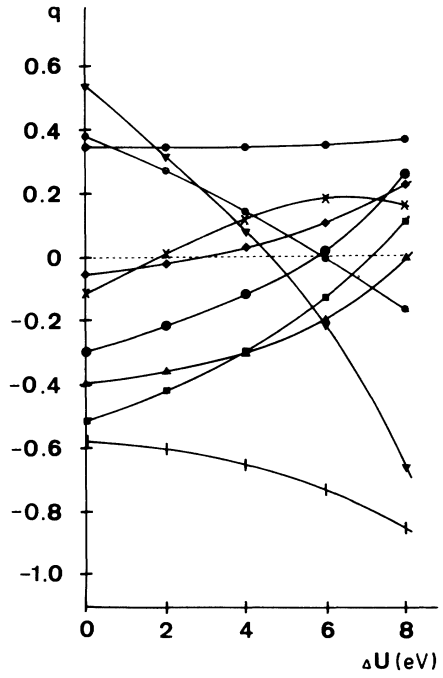

FIG. 5. Variation of the atomic net charges q_i in 11*b* as a function of ΔU. The labels of the q_i curves are explained in Fig. 4.

TABLE III. Band-structure data derived from the CO calculations on the *D-A* models. r_{DA} is the separation between the donor and acceptor in the various unit cells, α symbolizes the torsional angle between the functional groups. ΔU is the variation in the effective atomic-core potential in the carbonyl and hydroxyl groups. Band energies for the conduction bands (CB) and the valence bands (VB) are given at the zone center and the edge of the Brillouin zone. In the case of conducting polymers we have summarized the band energies of the overlapping bands. $\Delta\epsilon$ is the bandwidth which may differ from $|\epsilon(0)-\epsilon(\pi/c)|$. m_h is the effective mass for injected holes, while m_e is the effective mass for injected electrons. In the last columns, relevant data for the forbidden band gaps are summarized. ϵ_F symbolizes the Fermi energy (in eV) derived for conducting modifications of the *D-A* chains (10*b*).

r_{DA} Å	α	ΔU (eV)	$\epsilon(0)$ VB (eV)	$\epsilon(\pi/c)$ VB (eV)	$\Delta\epsilon$ VB (eV)	m_h	$\epsilon(0)$ CB (eV)	$\epsilon(\pi/c)$ CB (eV)	$\Delta\epsilon$ CB (eV)	m_e	Forbidden gap	Type of gap	Value of the k vector Top VB	Value of the k vector Bottom CB
3.0	0	0.0	−9.09	−9.03	0.69	3.8	−2.72	−1.93	0.78	3.4	6.31	indirect	π/c	0
		2.0	−8.95	−8.36	1.03	2.6	−1.83	−3.09	1.26	2.1	5.27	direct	π/c	π/c
		4.0	−8.76	−7.28	1.77	1.5	−2.42	−4.33	1.91	1.4	2.95	direct	π/c	π/c
		6.0	−8.31	−7.35	1.39	1.9	−2.66	−4.17	1.51	1.8	3.18	direct	π/c	π/c
		8.0	−7.48	−8.73	1.33	2.0	−2.44	−2.73	0.29	9.1	4.75	indirect	0	π/c
3.0	90°	0.0	−8.67	−9.41	0.94	2.8	−2.59	−1.88	0.44	6.0	6.08	direct	0	0
		2.0	−8.47	−9.11	0.79	3.3	−2.05	−3.09	1.05	2.5	5.38	indirect	0	π/c
		4.0	−8.19	−8.56	0.61	4.3	−2.73	−4.16	1.43	1.8	4.03	indirect	0	π/c
		6.0	−7.80	−7.86	0.38	7.0	−3.40	−5.49	2.09	1.3	2.31	indirect	0	π/c
		8.0	−7.59	−8.37	0.87	3.0	−3.59	−4.44	0.85	3.1	3.15	indirect	0	π/c
2.6	0°	0.0	−7.98	−10.03	2.05	1.5	−3.19	−2.17	1.02	3.0	4.79	direct	0	0
		2.0	−7.49	−9.82	2.33	1.3	−3.04	−2.02	1.03	3.0	4.45	direct	0	0
		4.0	−5.33	−4.03	1.50	2.0	−3.84	−9.02	5.17	0.6		$\epsilon_F=-5.0$		
		6.0	−5.67	−3.73	1.94	1.6	−4.07	−8.51	4.43	0.7		$\epsilon_F=-5.1$		
		8.0	−6.25	−7.66	1.44	2.1	−2.06	−2.78	0.89	3.4	3.47	indirect	0	π/c
2.6	90°	0.0	−7.28	−9.77	2.58	1.2	−4.49	−2.93	1.68	1.8	2.58	direct	$\pi/4.5c$	$\pi/4.5c$
		2.0	−7.14	−9.64	2.59	1.2	−4.40	−2.77	1.71	1.8	2.56	direct	$\pi/4.5c$	$\pi/4.5c$
		4.0	−6.97	−9.41	2.54	1.2	−4.32	−2.68	1.69	1.8	2.50	direct	$\pi/4.5c$	$\pi/4.5c$
		6.0	−6.69	−8.97	2.51	1.2	−4.36	−3.56	0.78	3.9	2.03	direct	$\pi/3c$	$\pi/3c$
		8.0	−7.02	−7.76	0.88	3.4	−3.45	−5.03	1.65	1.8	1.98	indirect	0	$\pi/1.2c$

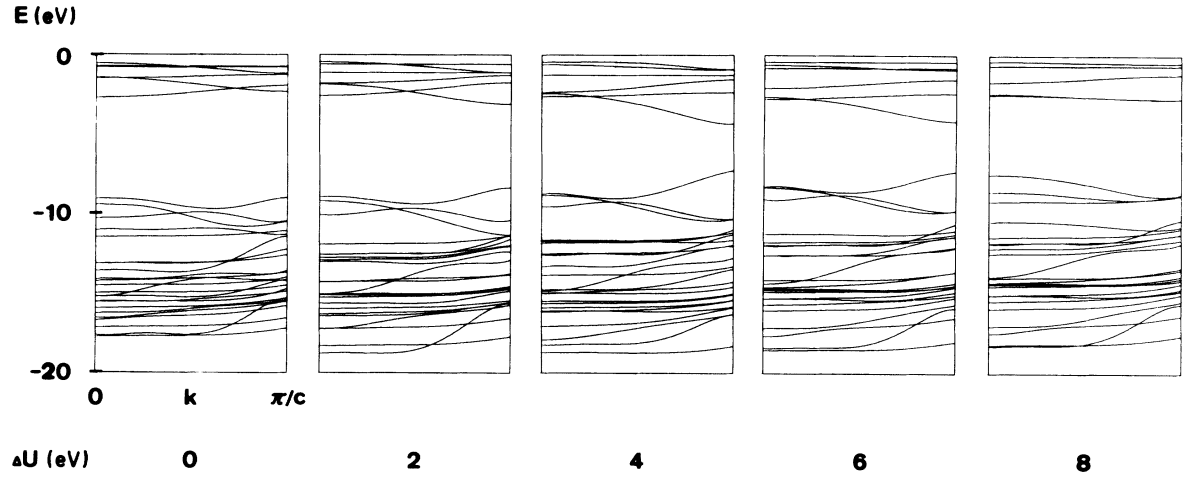

FIG. 6. Dispersion curves $\epsilon(k)$ of the 23 highest filled bands and the 6 lowest unfilled bands of 10*a* as a function of ΔU ($\Delta U=0$, 2, 4, 6, and 8 eV) according to the INDO CO method. The $\epsilon(k)$ curves are displayed in an interval between -20–0 eV.

boundary ($k=\pi/c$) states in the conduction band are hydroquinone functions. A reverse CT thus is found in 10*a* with the $\Delta U=6$-eV potential. The modified $\epsilon(k)$ shape in the $\Delta U=8$-eV model leads to a photon absorption that is prevailingly a local excitation in the donor units. It has been shown that the nature of the optical transitions in 10*a* depends strongly on the donor and acceptor capabilities of the active groups. Within the rather narrow ΔU limit encountered in the INDO CO calculations, a broad spectrum of absorption processes [local excitations, CT ($D\rightarrow A$) and reverse CT ($A\rightarrow D$), and mixtures from these excitation types] has been diagnosed.

The band gap in 11*a* (90°, 3 Å) is reduced in the ΔU interval $0\leq\Delta U\leq 6$ eV ($6.08\rightarrow 5.38\rightarrow 4.03\rightarrow 2.31$ eV) and is slightly enlarged in the last ($\Delta U=6\rightarrow\Delta U=8$ eV) step. A direct gap is only predicted for $\Delta U=0$ eV (center of the zone), the remaining $\epsilon(k)$ curves show an indirect forbidden gap that is between the zone center (top of the valence band) and the edge of the Brillouin zone (bottom of the conduction band). The effective masses (m_h, m_e) in 11*a* are enlarged in comparison to the 0° topology 10*a*. It is seen that the m_e numbers for injected electrons are closer to the free-electron limit.

Representative CO amplitudes ($\Delta U=0$, 4, and 8 eV) at the marginal k points are displayed in Fig. 12 for 11*a*. The direct photon absorption for the $\Delta U=0$ eV model corresponds to a transition from the dative to the no-bond structure of the *D-A* system. The following two model polymers with indirect gaps are characterized due to a superposition of the aforementioned excitation scheme accompanied by CT ($D\rightarrow A$) processes. The weak k depen-

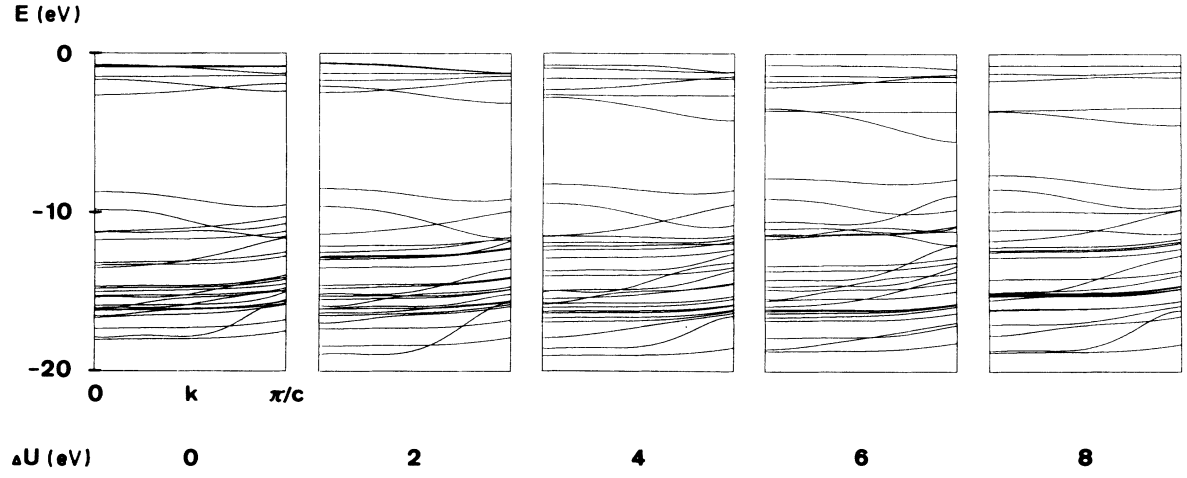

FIG. 7. Dispersion curves for the outer valence bands of 11*a* as a function of ΔU; see Fig. 6.

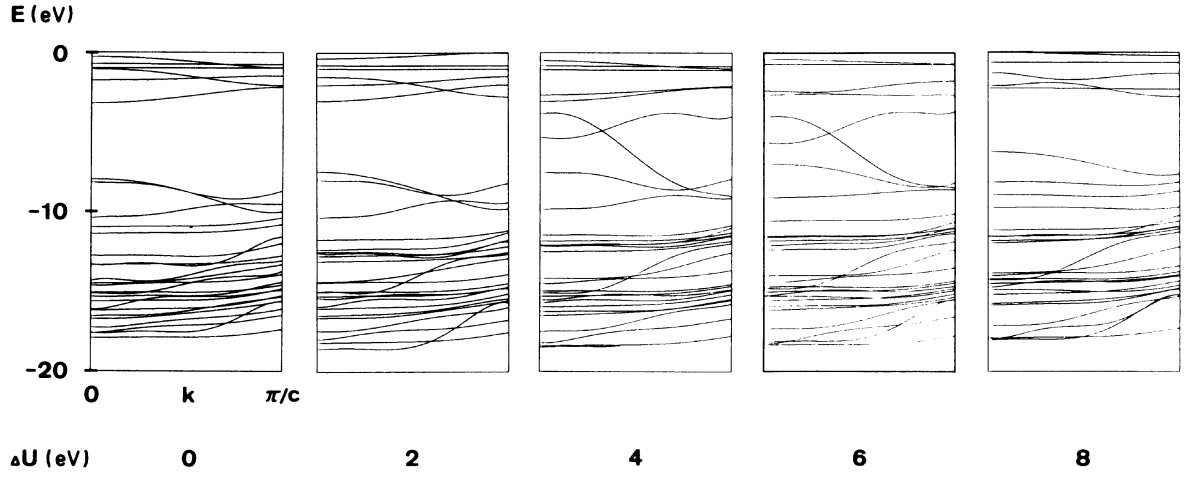

FIG. 8. Dispersion curves for the outer valence bands of 10*b* as a function of ΔU; see Fig. 6.

dence of the valence band in the $\Delta U = 6$ eV system facilitates the coexistence of indirect and direct photon absorptions. The direct gap opens a channel for a CT process from the donor to the acceptor (in contrast to 10*a* where reverse CT is diagnosed for the $\Delta U = 6$ eV potential), while the indirect band gap is characterized due to a superposition of CT and local excitations (acceptor). The $\Delta U = 8$ eV polymer 11*a* shows an $\epsilon(k)$ profile with states at the top of the valence band that have nonvanishing CO amplitudes in the *D* fragment, while the states at the bottom of the conduction band are localized in the donor. The absorption in the 1D stack is thus an intermixing of reverse CT transitions with local (donor) excitations. This behavior differs also significantly from the band-structure properties predicted for 10*a* ($\Delta U = 8$ eV).

The polymer model 10*b* (0°, 2.6 Å) shows an insulator-metal transition for intermediate ΔU values ($\Delta U = 4$–6 eV in the ΔU interval employed in Fig. 8). The band structure of 10*b* in the outer valence region between −20–0 eV is similar to the $\epsilon(k)$ shape derived for 10*a* for ΔU potentials of 0, 2, and 8 eV. The gap between the occupied and empty Fermi sea, however, is reduced in the phane model with the shorter *D-A* separation. The dispersion curves for ΔU values that lie between the interval displayed in Fig. 8 are shown in Fig. 13; the associated density-of-states profiles are given in Fig. 14.

The forbidden band gaps in 10*b* for ΔU values of 0, 2, and 8 eV are direct in the first two polymers (Γ point), but indirect in the model system with the largest variation in the donor and acceptor strength. The Fermi energies (ϵ_F) for the conducting modifications are found at about −5 eV, the $\epsilon(k)$ crossings are predicted in the region around $k \simeq \pi/3c$.

Representative CO amplitudes for 10*b* at the zone center and the edge of the Brillouin zone are collect-

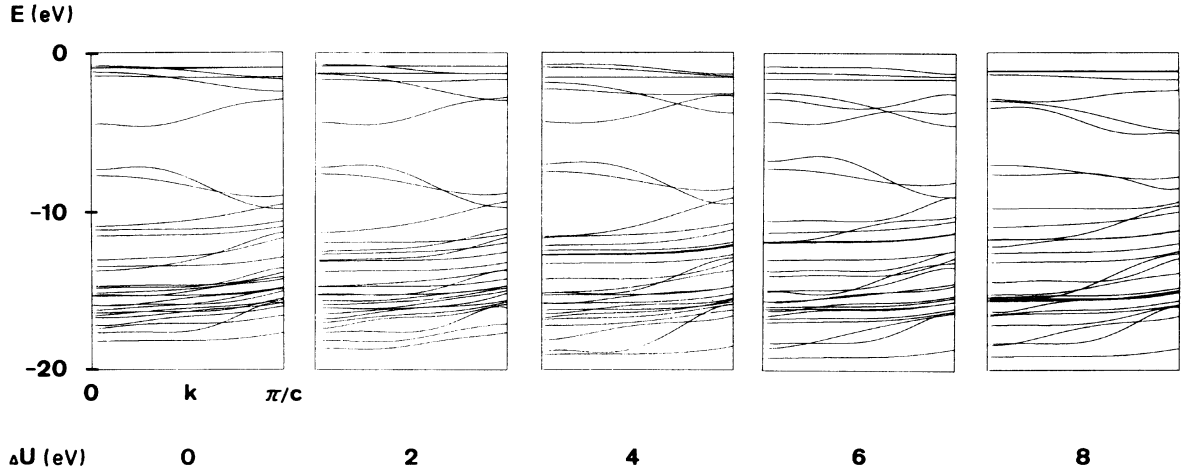

FIG. 9. Dispersion curves for the outer valence bands of 11*b* as a function of ΔU; see Fig. 6.

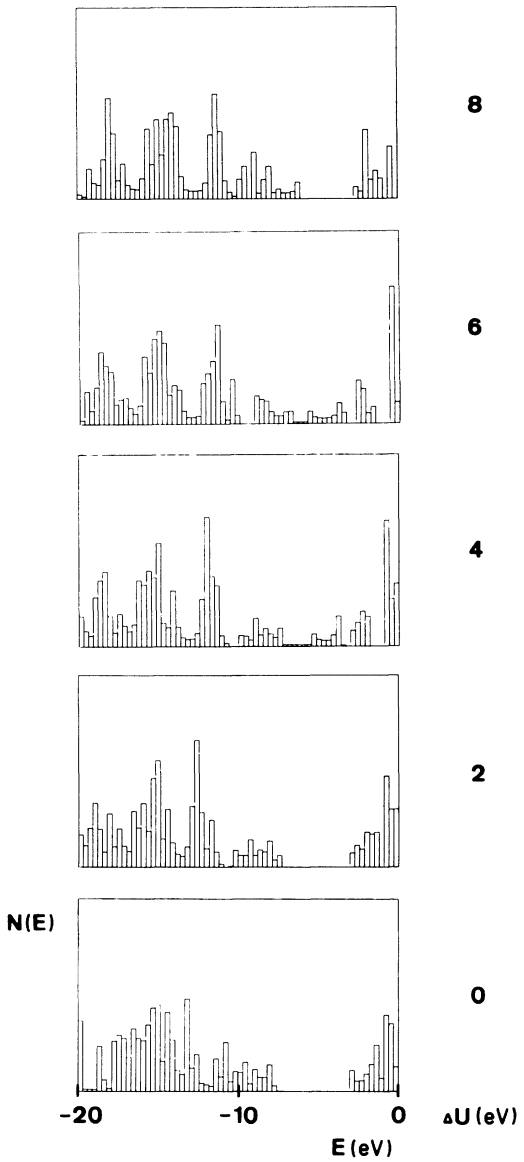

FIG. 10. Density of states $N(E)$ histograms for 10*b* as a function of ΔU. The states of all filled and unfilled bands in the interval between -20–0 eV have been taken into account in the determination of $N(E)$, while in the $\epsilon(k)$ representations (Figs. 6–9) a fixed number of energy bands has always been shown (the 23 highest filled ones as well as the 6 lowest empty bands). A common normalization factor has been employed for all $N(E)$ diagrams in this work. The energy grid for the sampling procedure amounts to 0.3 eV.

ed in Fig. 15. We have selected CO representations for ΔU elements of 0, 4, and 8 eV, respectively. It can be seen that the k dependence of the CO amplitudes in the valence and conduction bands is very weak (magnitude of the CO coefficients as a function of k), the Γ and X states are characterized by means of nearly identical CO wave functions. Comparable admixtures from both formal subunits (D and A) are predicted both at the center and the edge of the Brillouin zone (in contrast to 10*a*, where the states at the zone boundary are either localized in D or in A). The characteristic absorption for 10*b* in the vicinity of the standard parametrization of the CO Hamiltonian is thus a transition from the dative to the no-bond structure of the D-A polymer.

The CO amplitudes for states that belong to the crossing energy bands in conducting modifications of 10*b* cannot be correlated unambiguously with frontier orbitals of the separated molecular fragments. The schematic drawings in Fig. 15 demonstrate that various high-lying π functions from the occupied and virtual one-particle space are mixed into the corresponding band states of the 1D stack. The magnitude of the CO amplitudes is comparable in the donor and acceptor units, and depends only weakly on the value of the wave vector.

If ΔU exceeds a critical value ($\Delta U = 7$ eV), once again a 1D system with a finite band gap is predicted (metal-insulator transition). The indirect photon absorption ($\Gamma \rightarrow X$) is characterized due to a superposition of reverse CT processes ($A \rightarrow D$) and local excitations in the donor.

The theoretical results for 10*b* can be summarized as follows: The reduced D-A distance (intracell separation) in 10*b* leads to a stronger covalent interaction between one-electron functions localized in the donor and acceptor. The states at the top of the valence band (zone center) and at the bottom of the conduction band are out-of-phase (in-phase) combinations of occupied (empty) donor and acceptor functions. This splitting pattern leads to a close contact of $\epsilon(k)$ curves in the vicinity of the center of the Brillouin zone. If the donor and acceptor capabilities are enlarged, an allowed crossing of two $\epsilon(k)$ curves is predicted leading to a metallic state for the D-A polymer (first phase transition). The charge accumulation in the A units for extreme ΔU values then induces a crossover of the $\epsilon(k)$ curves that have an overlap in the conducting model polymers (second phase transition). One band is strongly stabilized; the other one, destabilized. The gradual variation of the $\epsilon(k)$ curves as a function of ΔU is clearly seen in Figs. 8 and 13.

An insulator-metal transition is not observed in the 90° system with the short D-A separation 11*b* (Fig. 9). The calculated forbidden band gaps span a range from 2.58 eV (standard parametrization) to 1.98 eV for $\Delta U = 8$ eV. With the exception of the last polymer model a direct gap is predicted. The k values for the minimum gap amount to $\pi/4.5c - \pi/3c$. An indirect gap is encountered in the polymer 11*b* with the ΔU potential of 8 eV. The

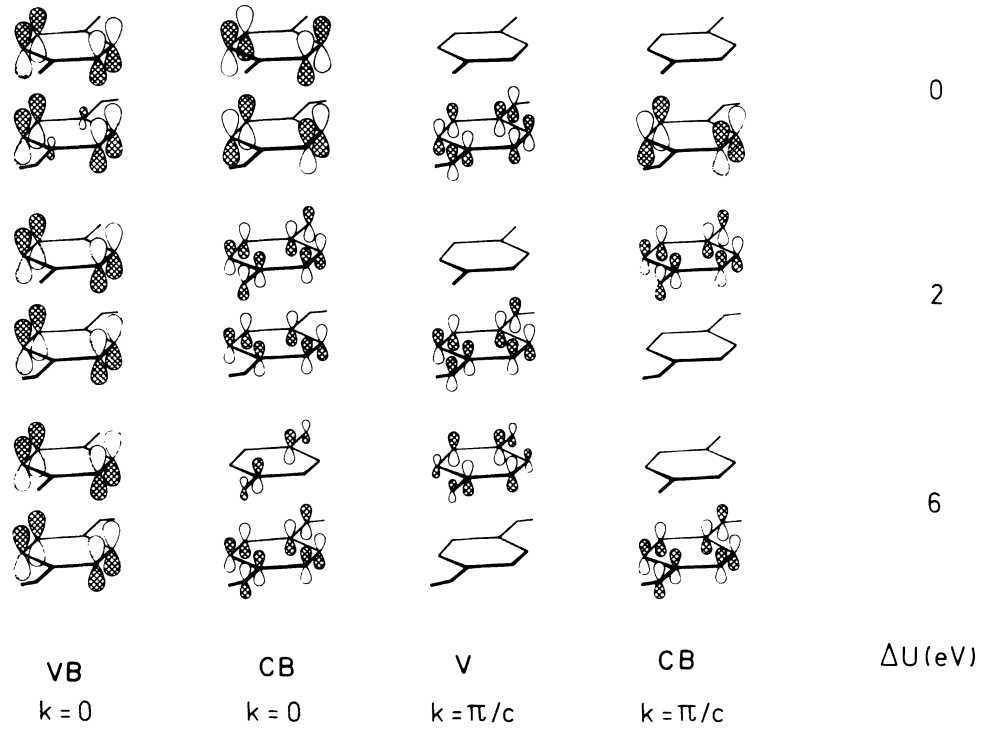

FIG. 11. Schematic representation of the CO amplitudes in the valence and conduction bands of 10*a* at the center of the Brillouin zone ($k=0$) and the edge of the zone ($k=\pi/c$). The CO wave functions are displayed for the following ΔU potentials: $\Delta U=0$ eV (top), $\Delta U=2$ eV (middle), $\Delta U=6$ eV (bottom). Only the most important CO admixtures are shown in the simplified diagram. VB represents the valence band, CB represents the conduction band.

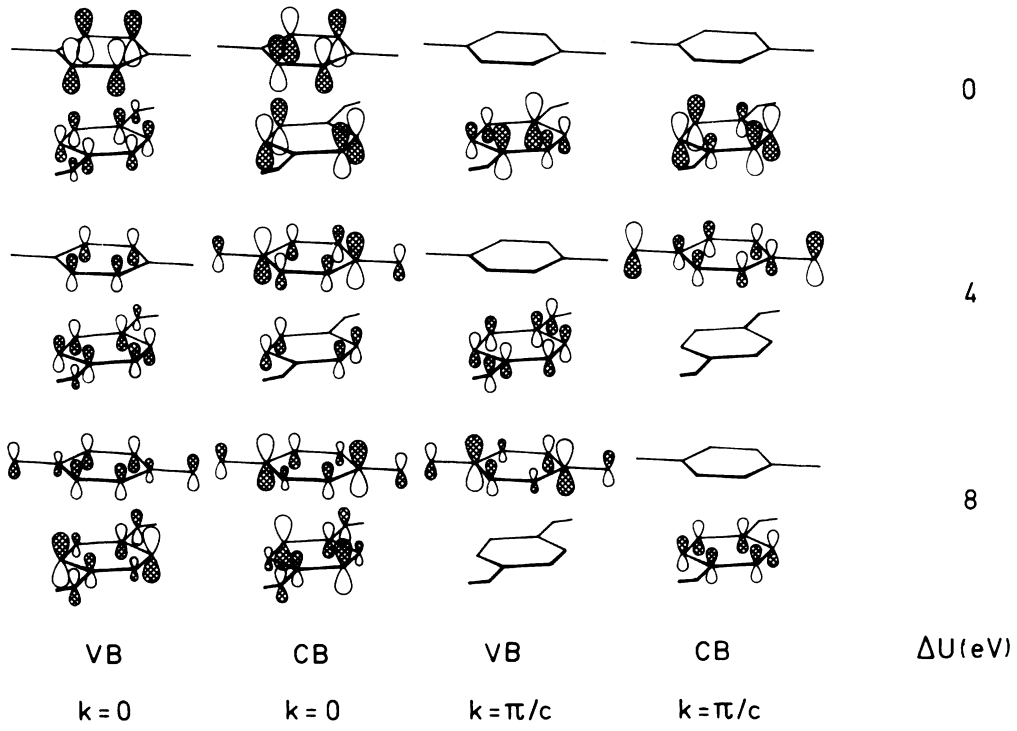

FIG. 12. Schematic representation of the CO amplitudes in the valence and conduction bands of 11*a* at the marginal k points $k=0$ and $k=\pi/c$. Top: $\Delta U=0$ eV; middle: $\Delta U=4$ eV; bottom: $\Delta U=8$ eV.

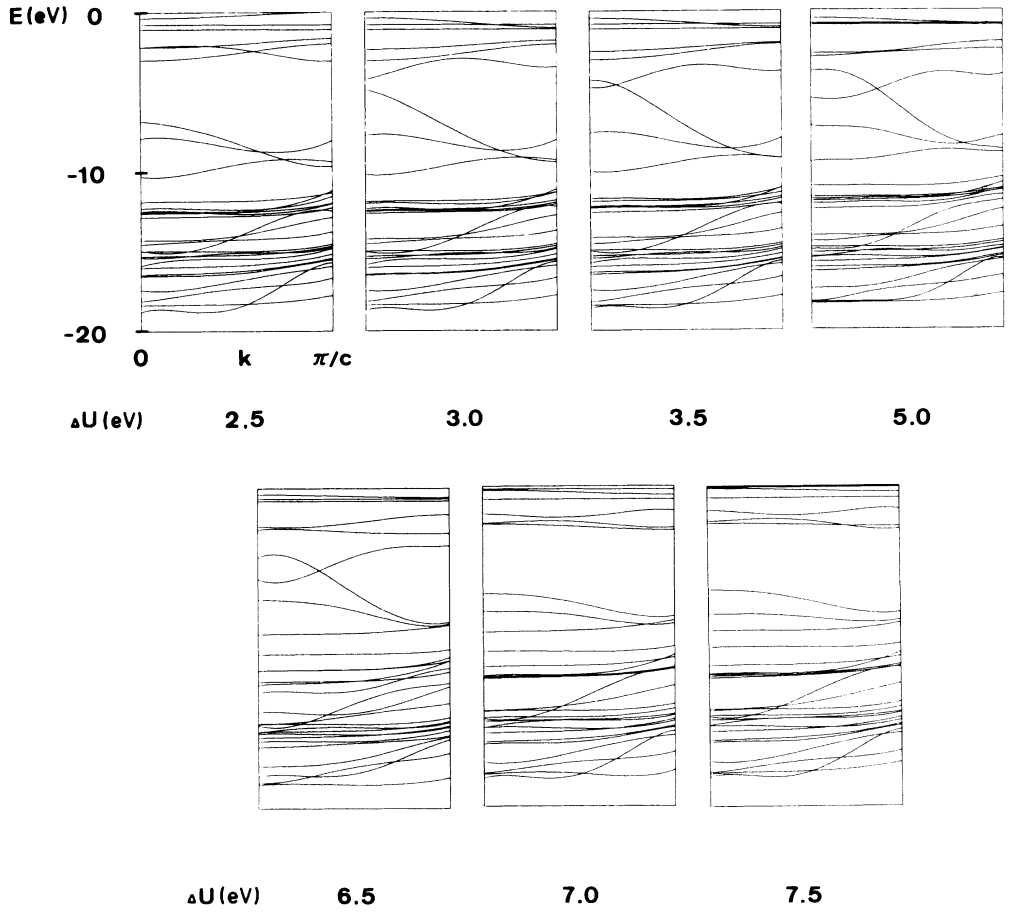

FIG. 13. Dispersion curves for the outer valence bands of some additional models of 10*b* as a function of ΔU; we have selected ΔU potentials that are not shown in the 2-eV grid of Fig. 8.

top of the valence band is predicted at the zone center, while the bottom of the conduction band is found at the marginal X point. The $\epsilon(k)$ curves in Fig. 9 demonstrate impressively that the finite gaps in 11*b* must be traced back to forbidden crossings of dispersion curves in k space. The effective masses for injected holes are near to the free-electron value (exception: $\Delta U = 8$ eV, $m_h = 3.4$), while the reduced bandwidth in the conduction bands leads to enlarged m_e parameters.

CO amplitudes for 11*b* at the Γ and X points are displayed schematically in Fig. 16. We have adopted the model polymers with $\Delta U = 0$ eV and $\Delta U = 8$ eV. It is seen that the conduction and valence bands belong to the same irreducible representation under C_2 symmetry. The states at the zone center in the valence band are out-of-phase linear combinations with comparable admixtures from the donor and acceptor moieties. The Γ states in the conduction band show an additive phase relation between the two π fragments within the unit cell of the 1D stack. The avoided curve crossing in the reciprocal k space is thus straightforwardly explained. In analogy to the model polymer 10*b* it is impossible to relate the states in the conduction and valence bands of 11*b* to definite one-electron functions of the *D* and *A* moieties. As a result of a strong intermixing between different donor and acceptor levels, CO's are derived that show new nodal properties. The CO amplitudes in 11*b* are determined due to strong deviations from the approximate mirror symmetry in the *D-A* polymers which is only slightly perturbed by means of the hydrogen atoms in the donor units. In the CO diagrams for the remaining 1D stacks localization properties are encountered that show only insignificant perturbations from the mirror symmetry, the CO amplitudes at the centers C_2/C_6, C_3/C_5 (donor), and C_{10}/C_{14} and C_{11}/C_{13} (acceptor) are nearly identical. The strong CO perturbation in 11*b* must be traced back to the fact that symmetry constraints are of larger importance in the vicinity of avoided crossing regions in k space. It is evident that an insulator-metal transition in *D-A* polymers with the 90° topology and short *D-A* distances

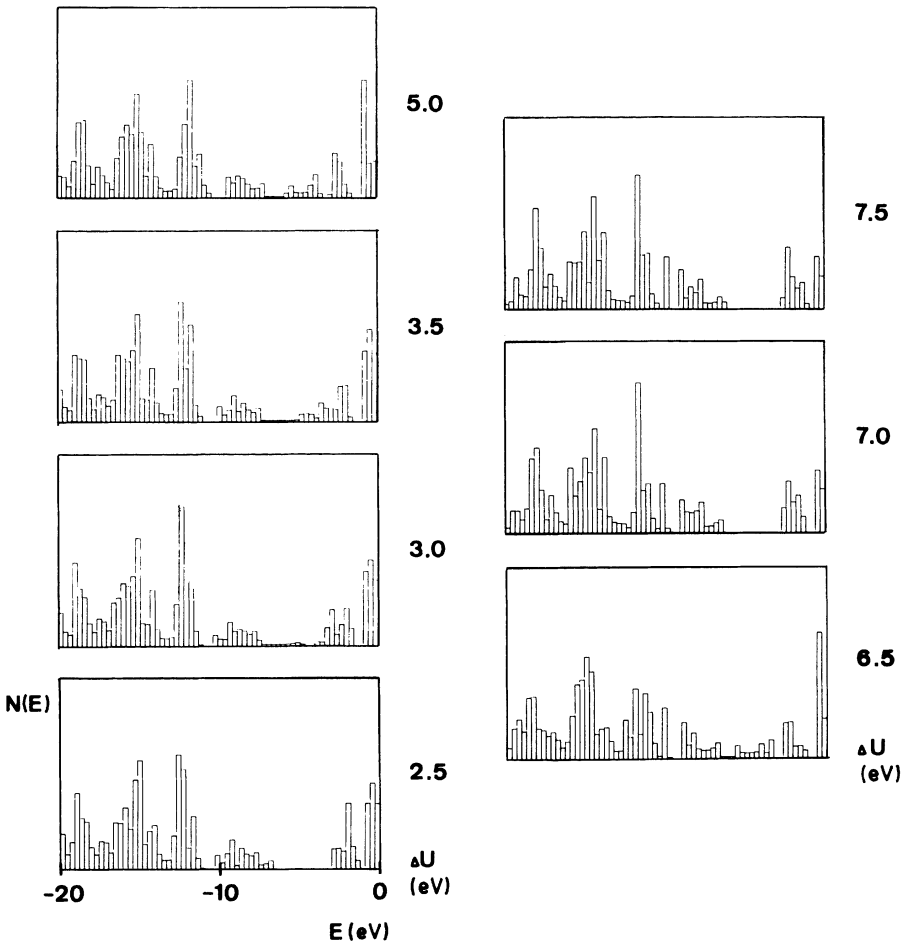

FIG. 14. Some additional density-of-states distributions in 10*b* as a function of ΔU. We have collected data points (ΔU) that are not shown in the 2-eV grid of Fig. 10. The $N(E)$ histograms are associated to the $\epsilon(k)$ curves of Fig. 13. In analogy to Fig. 10, all $\epsilon(k)$ states in the interval between -20—0 eV have been taken into account. The energy grid in the $N(E)$ plot amounts to 0.3 eV.

should be possible, if the solid-state symmetry is violated by means of unsymmetrical substitution patterns in the organic π systems. The photon absorption in the models with the direct band gaps leads to a transition from the dative structure of the polymer to the no-bond configuration ($0 \leq \Delta U \leq 6$ eV). In the indirect transition that is predicted for the system with the maximum ΔU potential ($\Delta U = 8$ eV), significant CT ($D \rightarrow A$) admixtures are encountered in the lowest excitation.

Detailed experimental studies on weakly coupled organic *D-A* systems have shown that the character (polarity, charge separation) of the excited states in the 1D stacks depends strongly on the specific donor and acceptor units that form the low-dimensional materials.[5,57] Highly polar and nearly unpolar excited states can be discriminated by means of the different transfer mechanisms for, e.g., excitons. The INDO CO studies on idealized models have shown that the character [localization properties, $\epsilon(k)$ shape] of the outer valence bands in *D-A* stacks can be significantly modified due to small electronic changes in the donor and acceptor fragments. In our model studies these differences have been simulated due to variable electronegativities in the active groups. The transposition to real systems requires electronic modifications due to substituents with electron donating or electron attracting properties, or due to new atomic species in the active donor or acceptor groups. Both operations lead to variations in the band energies.

The detailed analysis of the band-structure properties of the highest filled and lowest unfilled bands in the *D-A* models 10*a*—11*b* has shown that we have simulated theoretically all the ground-state and excited-state properties (in the framework of a model that corresponds to a regular infinite chain which is subject to cyclic boundary conditions) that

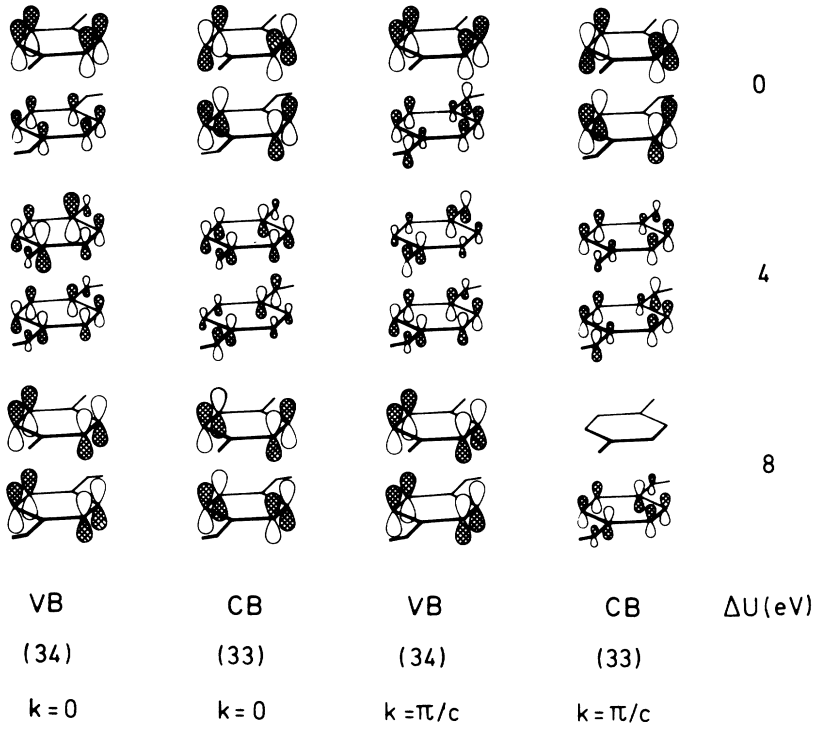

FIG. 15. Schematic representation of the CO amplitudes in the valence and conduction bands (overlapping bands in the conducting state of the polymer) of 10*b* at $k=0$ and $k=\pi/c$. Top: $\Delta U=0$ eV; middle: $\Delta U=4$ eV; bottom: $\Delta U=8$ eV. The model system with the $\Delta U=4$ eV potential is a conductor while finite band gaps are predicted for $\Delta U=0$ eV and $\Delta U=8$ eV.

have been verified in experimental investigations on "real" *D-A* stacks: (a) CT processes $D\rightarrow A$, where the polarity of the stack is enhanced in the excited state; (b) reverse CT processes and transitions from dative to no-bond structures that diminish the charge separation in the electronic ground state; (c) microstates in the *D-A* polymers which are distinguished due to CO amplitudes that are prevailingly localized either in *D* or in *A*; these localization properties are a necessary condition for excitations of the Frenkel type; (d) photon absorptions that correspond to a transition area between Frenkel-type and Wannier-type excitations; (e) strong $\epsilon(k)$ dependence as a function of the mutual *D-A* orientation (libration phenomena in weakly coupled *D-A* stacks).

The following important consequences can be deduced for the specific *D-A*-phane problem on the basis of the INDO CO studies with the variable

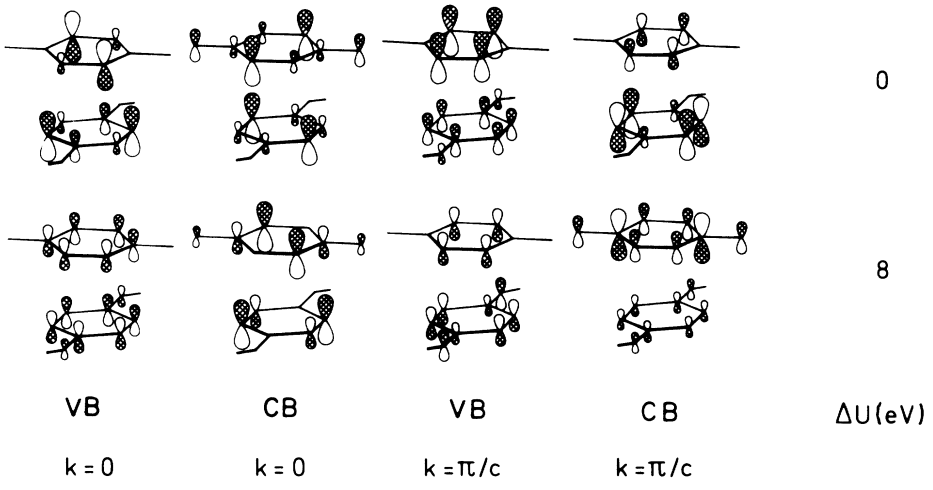

FIG. 16. Schematic representation of the CO amplitudes in the valence and conduction bands of 11*b* at $k=0$ and $k=\pi/c$. Top: $\Delta U=0$ eV; bottom: $\Delta U=8$ eV.

model Hamiltonian:

(i) The band gap (or the insulating versus metallic properties) of a *D-A* phane depends strongly on the mutual orientation of the donor and acceptor moieties and on the spacing between both fragments.

(ii) The gap is reduced with decreasing *D-A* separation in the phane. Suitable model systems are, therefore, compounds with a maximum number of bridging units (superphane). Increasing alkyl substitution in the conjugated organic π rings, however, prevents the insertion of donor or acceptor functions.

(iii) The covalent coupling between the donor and acceptor units can be strengthened by means of atomic centers with diffuse atomic orbitals in the case of a fixed *D-A* separation (B, Si, and Ge centers instead of C atoms). Such an exchange leads to an enhanced coupling for a constant *D-A* distance.

(iv) The forbidden band gap is smallest (possibility of an insulator-metal transition) for *D-A* phanes where the charge separations per unit cell amounts to ca. 1*e*; the gaps are enhanced if the donor and/or acceptor capabilities are furthermore enlarged.

(v) Two convenient functional donor and acceptor groups per π system are insufficient in [2.2] phanes to show semiconducting or conducting solid-state properties.

(vi) Pseudogeminal phane models are better precursors in comparison to pseudo-ortho orientations where avoided curve crossings have been diagnosed.

IV. OTHER SOLID-STATE MODELS FOR *D-A* PHANES

Instead of doing band-structure calculations one might try to treat *D-A* crystals as giant molecules[58] in the framework of a configuration interaction (CI) model in the space spanned by the four frontier orbitals of each *D-A* unit. Such a theoretical approach is indeed able to reproduce qualitatively the most important aspects of monomer *D-A* complexes or cyclophanes.[27] Recently this model has been used by Shaik[59] in order to discriminate between the physical properties of mixed and segregated arrangements of the donors and acceptors in *D-A* crystals.

However, this CI model is not applicable with nonvanishing CT interactions between the highest occupied molecular orbital (HOMO) of the donor and the lowest unoccupied molecular orbital (LUMO) of the acceptor as in 10*a* and 10*b*, since the lowest and highest eigenvalue of the CI matrix shift due to the lack of size consistency in CI procedures that are restricted to at most single excited configurations with respect to the no-bond function. In this state all the HOMO's of the donors and acceptors are doubly occupied.[60] In the following we want to symbolize the no-bond state as

$$\cdots (DA)_{i-1}(DA)_i(DA)_{i+1}\cdots .$$

Furthermore, this model is unable to reproduce the insulator-metal transition encountered for 10*b* because the dispersion must be traced back to the mixing of several high-lying π functions and not just to the frontier orbitals that are merged in the corresponding band states.

With vanishing CT interaction between the frontier orbitals of the donor and acceptor (e.g., 11*a* and 11*b*), the CI four-orbital model is no longer divergent. The model has been used in Ref. 59 for the study of segregated stacks of donors and acceptors. In addition to the no-bond state that determines the zero of the energy, the following configurations can be formulated within each *D-A* unit:

(i) The local excited configuration $C_{(\mathrm{LE})_i}$ which describes a mixed local excitation in the donor or the acceptor, respectively.[27] The corresponding energies are determined by the singlet excitations of the donor or the acceptor.

(ii) A charge-transfer configuration $C_{(\mathrm{CT})_i}$ whose energy decreases with increasing *D-A* abilities.[27]

These configurations can be visualized as

$$C_{(\mathrm{LE})_i} \equiv \cdots (DA)_{i-1}(DA)_i^*(DA)_{i+1}\cdots$$

and

$$C_{(\mathrm{CT})_i} \equiv (DA)_{i-1}(D^+A^-)_i(DA)_{i+1}\cdots .$$

There are many CT configurations CT_{ij} with an excitation from the donor in the jth unit to an acceptor in the unit j. However, only the CT configurations

$$\mathrm{C}_{(\mathrm{CT})_{i+1,i}} \equiv \cdots (DA^-)_i(D^+A)_{i+1}\cdots$$

are of interest as it can be shown that the following configurations are coupled by taking into account only the nearest-neighbor interaction:

$$\cdots C_{(\mathrm{CT})_i} \leftrightarrow C_{(\mathrm{LE})_i} \leftrightarrow C_{(\mathrm{CT})_{i+1,i}} \leftrightarrow C_{(\mathrm{LE})_{i+1}} \leftrightarrow C_{(\mathrm{CT})_{i+1}} \cdots .$$

The energies of these $C_{(\mathrm{CT})_{i+1,i}}$ configurations are higher than those of the $C_{(\mathrm{CT})_i}$ excitations.

If the mutual *D-A* interaction is large enough one obtains besides the no-bond state a low-lying band where the $C_{(\mathrm{CT})_i}$ configurations are weakly coupled to the $C_{(\mathrm{LE})_i}$ and $C_{(\mathrm{CT})_{i+1,i}}$ configurations. This can be visualized as

$$[\cdots (DA)_i(DA)_{i+1}\cdots]+c_1[\cdots (DA^-)_i(D^+A)_{i+1}\cdots]+c_2[\cdots (DA)_i^*(DA)_{i+1}\cdots]+\cdots ,$$

with small mixing coefficients c_1,c_2. If this low-lying band overlaps with the no-bond state one can consider the migration of a mobile excess electron injected into the no-bond state by virtue of a supertransfer involving CT states[24]:

$$\cdots (DA^-)_i(DA)_{i+1}\cdots \xrightarrow{c_{(CT)_i}} \cdots (DA^-)_i(D^+A^-)_{i+1}\cdots \xrightarrow{c_{(CT)_{i+1,i}}} \cdots (DA)_i(DA^-)_{i+1}\cdots .$$

On the other hand, the results of the present INDO CO study show that this simplified model is most probably not a physically realistic description for the low-dimensional systems, in contrast to their application to monomer *D-A* systems, because it does not take into account the often dramatical changes in the shape of the dispersion curves and the nodal properties of the band states in the 1D stack (e.g., 11*b*).

V. CONCLUSION

The band structures of two *D-A* stacks, 10 and 11, have been studied by means of the CO formalism based on the tight-binding approximation; computational framework for the CO procedure was a semiempirical INDO model. The solid-state properties of the *D-A* polymers have been examined as a function of the distance and the mutual orientation between the donor and acceptor units, and as a function of the effective donor and acceptor capabilities. The latter quantities have been modified by means of the atomic basis energies in the carbonyl and hydroxyl groups of 10 and 11. The employed geometries for the theoretical approach have been selected on the basis of known data for experimentally feasible *D-A* phanes.

It has been shown that the band-structure properties can be dramatically modified by means of small variations either in the geometry of the stacks or due to the strength of the *D-A* pairs. It has been verified that electronic solid-state effects (k-vector dependence) in the 1D systems are often so important that molecular models derived for finite *D-A* units can be adopted only with great care. The character of the band states in the valence and conduction bands of the 1D systems depends critically on the value of the k vector in the solid state. In contrast to simple molecular suggestions it has been demonstrated that the states at the top of the valence band and the bottom of the conduction band are distinguished by CO amplitudes which show on one side strong *D-A* intermixing but also vanishing contributions from one fragment (*D* or *A*) for small "perturbations." Additionally, localization properties have been detected that lead to reverse CT processes. Small variations in the donor or acceptor units often cause substantial modifications in the corresponding band structures, a necessary condition for phase transitions (e.g., insulator-metal transition) in the solid state.

The INDO CO data derived for the model polymers 10 and 11 offer deep insight into the factors that are the physical origin for the large variety of solid-state properties encountered in low-dimensional *D-A* stacks (e.g., polarity in the ground and excited states, nature of the charge-carrier processes, local versus delocalized excitations, migrations of local excitations within the donor or acceptor manifold due to the localization properties of microstates in the various bands, etc.). It is our opinion that band-structure calculations on realistic *D-A* models are a suitable tool to understand and to explain basic principles of the electronic structure of *D-A* stacks in the solid state, while highly sophisticated analytical approaches that are restricted to extremely small unit-cell dimensions (one or two orbitals per cell), indeed allow thorough formal descriptions of the systems, but where a large amount of quantum chemical information has been omitted.

ACKNOWLEDGEMENTS

This work has been supported by the Stiftung Volkswagenwerk (M.C.B.), by the Fonds der Chemie, and by the Deutsche Forschungsgemeinschaft (H.V.).

[1]H. M. McConnell, B. M. Hoffman, and R. M. Metzger, Proc. Natl. Acad. Sci. USA 53, 46 (1965); Z. G. Soos, Annu. Rev. Phys. Chem. 25, 121 (1974).

[2]*Chemistry and Physics of One-Dimensional Metals,* edited by H. J. Keller (Plenum, New York, 1977); Z. G. Soos and D. J. Klein, in *Molecular Association,* edited by R. Foster (Academic, New York, 1975), Vol. 1, p. 1.

[3]*Physics and Chemistry of Low-Dimensional Solids,* edited by L. Alcazer (Plenum, New York, 1980); *Quasi-One-Dimensional Conductors II,* Vol. 96 of *Lecture Notes in Physics,* edited by S. Barišić, A. Bjeliš, and J. R. Cooper (Springer, Berlin, 1979).

[4]R. Foster, J. Phys. Chem. 84, 2135 (1980).

[5]H. Möhwald, Phys. Bl. 35, 617 (1979).

[6]W. Rebafka and H. A. Staab, Angew. Chem. 85, 831 (1973); 86, 234 (1974).
[7]H. A. Staab and W. Rebafka, Chem. Ber. 110, 3333 (1977).
[8]H. A. Staab and V. Taglieber, Chem. Ber. 110, 3366 (1977).
[9]H. A. Staab and H.-E. Henke, Tetrahedron Lett. 1955 (1978); R. Reimann and H. A. Staab, Angew. Chem. 90, 385 (1978); H. A. Staab, J. Ippen, C. Tao-pen, C. Krieger, and B. Starker, *ibid.* 92, 49 (1980); H. A. Staab and W. K. Appel, Justus Liebigs Ann. Chem. 1065 (1981).
[10]H. A. Staab and V. Schwendemann, Angew. Chem. 90, 805 (1978); Justus Liebigs, Ann. Chem. 1258 (1979).
[11]T. E. Peacock and R. McWeeny, Proc. Phys. Soc. London 74, 385 (1958).
[12]G. del Re, J. Ladik, and G. Biczo, Phys. Rev. 155, 997 (1967); J. M. André, L. Gouverneur, and G. Leroy, Int. J. Quantum Chem. 1, 451 (1967).
[13]J. Hubbard, Proc. R. Soc. London. Ser. A 276, 238 (1963); 277, 237 (1964); 281, 401 (1964); 285, 542 (1965).
[14]G. Beni and P. Pincus, Phys. Rev. B 9, 2963 (1974); J. F. Kwak and G. Beni, *ibid.* 13, 674 (1976); J. Hubbard, *ibid.* 17, 494 (1978).
[15]W. P. Su, J. R. Schrieffer, and A. J. Heeger, Phys. Rev. Lett. 42, 1698 (1979); Phys. Rev. B 22, 2099 (1980).
[16]S. Mazumdar and Z. G. Soos, Synth. Met. 1, 77 (1979); S. R. Bondeson and Z. G. Soos, J. Chem. Phys. 71, 3807 (1979); 44, 403 (1979).
[17]S. Mazumdar and Z. G. Soos, Phys. Rev. B 23, 2810 (1981); D. J. Klein and Z. G. Soos, Mol. Phys. 20, 1013 (1971).
[18]A. Karpfen, J. Ladik, G. Stollhoff, and P. Fulde, Chem. Phys. 8, 215 (1975); J. Ladik, Int. J. Quantum Chem. Symp. 9, 1563 (1975).
[19]R. D. Singh and J. Ladik, Phys. Lett. 65A, 264 (1978).
[20]S. Suhai, Solid State Commun. 21, 117 (1977); Phys. Lett. 62A, 185 (1977); S. Suhai and G. Biczo, Phys. Lett. 62A, 380 (1977).
[21]S. Suhai and J. Ladik, Phys. Lett. 77A, 25 (1980).
[22]Z. G. Soos and S. Mazumdar, Phys. Rev. B 18, 1991 (1978).
[23]Z. G. Soos, S. R. Bondeson, and S. Mazumdar, Chem. Phys. Lett. 65, 331 (1979).
[24]P. Petelenz, Chem. Phys. Lett. 47, 603 (1977); P. Petelenz and T. Zyczkowska, *ibid.* 67, 149 (1979).
[25]P. Petelenz and B. Petelenz, Phys. Status Solidi B 81, 49 (1977); P. Petelenz *ibid.* 83, 169 (1977); 88, 689 (1978); 90, 635 (1978).
[26]T. Otha, H. Kuroda, and T. L. Kunii, Theor. Chim. Acta 19, 167 (1970); Z. Yoshida and T. Kobayashi, *ibid.* 23, 67 (1972); B. Mayoh and C. K. Prout, J. C. S. Faraday II 68, 1072 (1972); H. Vogler, Theor. Chim. Acta 60, 65 (1981).
[27]H. Vogler, Croat. Chem. Acta (in press); H. Vogler and M. C. Böhm, Mol. Phys. (in press).
[28]F. Cavallone and E. Clementi, J. Chem. Phys. 63, 4304 (1975).
[29]I. Goldberg, Theor. Chim. Acta 40, 271 (1975).
[30]B. D. Silvermann, Chem. Phys. Lett. 59, 143 (1978).
[31]R. S. Mulliken, J. Am. Chem. Soc. 74, 811 (1952); J. Chem. Phys. 56, 801 (1952); R. S. Mulliken and W. B. Person, *Molecular Complexes: A Lecture and Reprint Volume* (Wiley, New York, 1969); R. Foster, *Organic Charge Transfer Complexes* (Academic, London, 1969).
[32]E. Heilbronner and J. P. Maier, Helv. Chim. Acta 57, 151 (1974); B. Kovač, M. Mohraz, E. Heilbronner, V. Boekelheide, and H. Hopf, J. Am. Chem. Soc. 102, 4314 (1980), and references cited therein; T. Geiger, H. A. Staab, and H. Vogler (unpublished).
[33]R. Hoffmann, Acc. Chem. Res. 4, 1 (1969); R. Gleiter, Angew. Chem. 86, 770 (1974).
[34]K. Lonsdale, J. J. Milledge, and K. V. K. Rao, Proc. R. Soc. London Ser. A 255, 82 (1960); H. Hope, J. Bernstein, and K. N. Trueblood, Acta Crystallogr. B 28, 1733 (1972).
[35]A. W. Hanson and M. Röhrl, Acta Crystallogr. B 28, 2032 (1972); A. W. Hanson, *ibid.* 33, 2003 (1977).
[36]A. W. Hanson and T. S. Cameron, J. Chem. Res. (S) 336 (1980).
[37]M. C. Böhm, Theor. Chim. Acta 62, 351 (1983).
[38]M. C. Böhm and R. Gleiter, Theor. Chim. Acta 59, 127 (1981); 59, 153 (1981).
[39]J. Koutecký, J. Čižek, J. Dubsky, and K. Hlavaty, Theor. Chim. Acta 2, 462 (1964); J. Koutecký, J. Chem. Phys. 47, 1051 (1967).
[40]J. Čižek, J. Chem. Phys. 45, 4256 (1966); J. Čižek, J. Paldus, and I. Hubac, Int. J. Quantum Chem. 8, 951 (1974); J. Paldus *ibid.* S 8, 293 (1974).
[41]A. Pellegatti, J. Čižek, and M. Paldus, J. Chem. Phys. 60, 4825 (1974); M. Saute, J. Paldus, and J. Čižek, Int. J. Quantum Chem. 15, 463 (1979).
[42]K. Schulten, I. Ohmine, and M. Karplus, J. Chem. Phys. 64, 4422 (1976); I. Ohmine, M. Karplus, and K. Schulten *ibid.* 68, 2298 (1978).
[43]B. Dick and G. Hohlneicher, Theor. Chim. Acta 53, 221 (1979).
[44]M. C. Böhm, Ber. Bunsenges. Phys. Chem. 86, 56 (1982); Int. J. Quantum Chem. 22, 939 (1982).
[45]M. C. Böhm, Chem. Phys. 67, 255 (1982).
[46]J. M. Sichel and M. A. Whitehead, Theor. Chim. Acta 11, 220 (1968); L. Di Sipio, E. Tondello, G. De Michelis, and L. Oleari, Chem. Phys. Lett. 3, 287 (1971).
[47]M. J. S. Dewar and N. L. Hojvat(Sabelli), J. Chem. Phys. 34, 1232 (1961); Proc. R. Soc. London Ser. A 264, 431 (1961); J. Phys. Chem. 66, 2310 (1962); K. Ohno, Theor. Chim. Acta 3, 219 (1964); G. Klopman, J. Am. Chem. Soc. 86, 4550 (1964).
[48]J. Delhalle, in *Electronic Structure of Polymers and Molecular Crystals,* edited by J. M. André and J. Ladik (Plenum, New York, 1975), p. 53.
[49]J. Brust, in *Methods in Computational Physics,* edited by B. Alder, S. Fernbach, and M. Rothenberg (Academic, New York, 1968), Vol. 8, p. 33.
[50]C. Krieger and H. A. Staab (unpublished).
[51]L. E. Sutton, *Tables of Interatomic Distances and Configuration in Molecules and Ions,* Spec. Pub. No. 18

(The Chemical Society, London, 1965).
[52]N. W. Ashcroft and N. D. Mermin, *Solid State Physics* (Holt, Rinehart and Winston, New York, 1976).
[53]J. Ladik, in *Quantum Theory of Polymers,* edited by J.-M. André, J. Delhalle, and J. Ladik (Reidel, Dordrecht, 1978), p. 257.
[54]H. P. Kelly, Adv. Chem. Phys. 14, 129 (1969); W. Hunt and W. A. Goddard, Chem. Phys. Lett. 3, 414 (1969).
[55]J. C. Slater, *Quantum Theory of Molecules and Solids* (McGraw-Hill, New York, 1974), Vol. 4, p. 4.
[56]R. S. Mulliken, J. Chem. Phys. 23, 1833 (1955).
[57]H. Möhwald and E. Sackmann, Solid State Commun. 15, 445 (1974); Chem. Phys. Lett. 21, 43 (1973); Z. Naturforsch. 29a, 1216 (1974).
[58]A. Julg, in *Crystals as Giant Molecules,* Vol. 9 of *Lecture Notes in Chemistry* (Springer, Berlin, 1978).
[59]S. S. Shaik, J. Am. Chem. Soc. 104, 5328 (1982).
[60]T. Sakata and S. Nagakura, Bull. Chem. Soc. Jpn. 43, 1346 (1970).